Nonlocal Kondo effect and quantum critical phase in heavy-fermion metals

Jiangfan Wang[1] and Yi-feng Yang[1,2,3,*]

[1]*Beijing National Laboratory for Condensed Matter Physics, Institute of Physics, Chinese Academy of Science, Beijing 100190, China*
[2]*School of Physical Sciences, University of Chinese Academy of Sciences, Beijing 100190, China*
[3]*Songshan Lake Materials Laboratory, Dongguan, Guangdong 523808, China*

(Received 5 September 2020; revised 27 August 2021; accepted 27 September 2021; published 11 October 2021)

Heavy-fermion metals typically exhibit an unconventional quantum critical point or quantum critical phase at zero temperature due to the competition of the Kondo effect and magnetism. Previous theories were often based on certain local types of assumptions, and a fully consistent explanation of experiments has not been achieved. Here we develop an efficient algorithm for the Schwinger boson approach to explore the effect of spatial correlations on the Kondo lattice, and we introduce the concept of a nonlocal Kondo effect in the quantum critical region with deconfined spinons. We predict a global phase diagram containing a non-Fermi liquid quantum critical phase with a hidden holon Fermi surface and a partially enlarged electron Fermi surface for strong quantum fluctuations but a single quantum critical point for weak quantum fluctuations. This explains the unusual metallic spin liquid recently reported in the frustrated Kondo lattice CePdAl and resolves the Fermi volume puzzle in $YbRh_2Si_2$. Our theory highlights the importance of nonlocal physics and provides a unified understanding of heavy-fermion quantum criticality.

DOI: 10.1103/PhysRevB.104.165120

The interplay of antiferromagnetic (AFM) transition and f electron delocalization underlies many exotic properties of Kondo lattice physics [1,2]. In particular, the recent discovery of a non-Fermi liquid (NFL) quantum critical phase in the frustrated Kondo lattice CePdAl has posed an urgent challenge to clarify the nature of this intermediate state [3], which is in stark contrast to the usual observation of a single quantum critical point (QCP) in many heavy-fermion antiferromagnets, such as $YbRh_2Si_2$ [4–7], $CeRhIn_5$ [8,9], and $CeCu_{6-x}Au_x$ [10–13]. In the latter case, the AFM QCP is often thought to be accompanied by the full delocalization of f electrons into a heavy Fermi liquid (HFL), possibly manifested by an abrupt change in the electron Fermi surface from "small" (no f electrons) to "large" (with f electrons). In CePdAl, however, the two transitions are detached. The intermediate phase spans over a broad range of the pressure-magnetic field phase diagram and is neither magnetically ordered nor a Fermi liquid. A similar intermediate phase was observed previously in Ir- or Ge-doped $YbRh_2Si_2$ [14,15]. Its origin is unclear but is often attributed to magnetic frustrations, low dimensionality, or large spin/orbital degeneracy [16–19].

The lack of a thorough microscopic understanding lies in the extreme difficulty of simulating the Kondo lattice. The widely used dynamical mean-field theory [20] and its cluster extensions [21,22] can well capture local or short-range correlations but fail to describe long-range quantum critical fluctuations. Exact lattice simulations often require extensive computational efforts and can be applied only under very special conditions on small lattices [23]. In this regard, the recent development of the large-N Schwinger boson approach represents an important advance [24–29]. Compared to the prevalent slave-boson method, the Schwinger boson representation of spins allows for better treatment of local moment antiferromagnetism and its interplay with Kondo screening. However, its latest implementations on the Kondo lattice have all predicted direct transitions between antiferromagnetism and HFL, showing no sign of an intermediate phase [28,29].

The discrepancy comes from the local approximation adopted in these calculations, which ignores the momentum dependence of quasiparticle self-energies in order to reduce the computational efforts [28,29]. To overcome this issue, we go beyond the local approximation and develop an efficient numerical algorithm to solve the Schwinger boson self-consistent equations with full frequency and momentum-dependent self-energies. This enables us to study the low-energy charge and spin dynamics with both temporal and spatial fluctuations. Our method is then applied to the two-dimensional (2D) Kondo-Heisenberg model on the square lattice and finds, in a certain parameter range, an emergent intermediate state with gapless spinon and holon excitations and a partially enlarged (or "medium") electron Fermi surface due to the generalized Luttinger sum rule [30,31], which is forbidden in the local approximation. The phase diagram and finite-temperature properties are controlled by the interplay of a deconfined AFM QCP and a transition to the large electron Fermi surface, which merge together into a single transition for large spin size. Our key finding is a nonlocal Kondo effect mediated by holons propagating on the lattice. Our results explain the recent experiments in CePdAl and $YbRh_2Si_2$ and provide a unified theory of heavy-fermion quantum criticality.

*yifeng@iphy.ac.cn

We start with the following Hamiltonian:

$$H = t\sum_{\langle ij\rangle} c^\dagger_{i\alpha a} c_{j\alpha a} + J_K \sum_i \mathbf{S}_i \cdot \mathbf{s}_i + J_H \sum_{\langle ij\rangle} \mathbf{S}_i \cdot \mathbf{S}_j, \quad (1)$$

where $c^\dagger_{i\alpha a}$ creates a conduction electron of spin α and channel (orbital) $a = 1, 2, \ldots, K$ on site i, $\mathbf{s}_i$ is its spin operator, and $\mathbf{S}_i$ denotes the local spin. The Schwinger boson approach enlarges the SU(2) spin group to the symplectic group Sp(N) such that $\mathbf{S}_i \to S^{\alpha\beta}_i = b^\dagger_{i\alpha} b_{i\beta} - \tilde{\alpha}\tilde{\beta} b^\dagger_{i,-\beta} b_{i,-\alpha}$, where $b_{i\alpha}$ represents the Schwinger boson (spinon), $\alpha = \pm 1, \ldots, \pm N/2$, and $\tilde{\alpha} = \mathrm{sgn}(\alpha)$ [32]. A local constraint is then imposed to reduce the enlarged Hilbert space to physical subspace, $n_{b,i} \equiv \sum_\alpha b^\dagger_{i\alpha} b_{i\alpha} = 2S$, which may be implemented by introducing the Lagrange multiplier, $\sum_i \lambda_i (n_{b,i} - 2S)$. A biquadratic exchange term, $-\zeta J_H \sum_{\langle ij\rangle} (\mathbf{S}_i \cdot \mathbf{S}_j)^2$, is often included to avoid artificial first-order transitions at large N, which can be absorbed into the quadratic term under SU(2) symmetry [33]. Depending on the ratio of $2S/K$, three distinct regions exist where the local spins are underscreened ($2S/K > 1$), overscreened ($2S/K < 1$), or exactly screened ($2S/K = 1$) [34]. We focus on the exactly screened case. The Kondo and Heisenberg terms can be factorized using two auxiliary fields:

$$\frac{J_K}{N} S^{\alpha\beta}_i c^\dagger_{i\beta a} c_{i\alpha a} \to \frac{1}{\sqrt{N}} b^\dagger_{i\alpha} c_{i\alpha a} \chi_{ia} + \mathrm{H.c.} + \frac{|\chi_{ia}|^2}{J_K},$$

$$\frac{J_H}{N} S^{\alpha\beta}_i S^{\beta\alpha}_j \to \tilde{\alpha} b^\dagger_{j,-\alpha} b^\dagger_{i,\alpha} \Delta_{ij} + \mathrm{H.c.} + \frac{N|\Delta_{ij}|^2}{J_H}, \quad (2)$$

where Δ_{ij} denotes the spin-singlet valence bond on adjacent sites and $\chi^\dagger_{ia}$ can be viewed as a composite fermion of the Kondo state formed by a conduction hole and a spinon. $\chi^\dagger_{ia}$ is also called the holon field since it carries a positive electric charge and has no spin.

To proceed, we assume the mean-field variables $\lambda_i = \lambda$ and $\Delta_{i,i+\hat{x}} = \Delta_{i,i+\hat{y}} = \Delta$. The former replaces the local constraint $n_{b,i} = 2S$ by the average spinon occupation, and the latter describes a candidate spin liquid energetically favored in the Heisenberg model [35]. The rotational symmetry is preserved under combined operation of lattice rotation and gauge transformation [36]. In the large-N limit, the spinon and holon self-energies are [37]

$$\Sigma_b(\mathbf{p}, i\nu_n) = -\frac{\kappa}{\beta\mathcal{V}} \sum_{\mathbf{k}m} g_c(\mathbf{p}-\mathbf{k}, i\nu_n - i\omega_m) G_\chi(\mathbf{k}, i\omega_m),$$

$$\Sigma_\chi(\mathbf{p}, i\omega_m) = \frac{1}{\beta\mathcal{V}} \sum_{\mathbf{k}n} g_c(\mathbf{k}-\mathbf{p}, i\nu_n - i\omega_m) G_b(\mathbf{k}, i\nu_n), \quad (3)$$

where g_c is the bare Green's function of conduction electrons; G_b and G_χ are the full Green's functions of spinons and holons, which will be self-consistently determined by their self-energies; ω_m (ν_n) are the fermionic (bosonic) Matsubara frequencies; β is the inverse temperature; and $\mathcal{V}$ is the total number of lattice sites. The parameter $\kappa \equiv 2S/N = K/N$ controls the effective strength of quantum fluctuations. The self-energy of conduction electrons is absent in the large-N limit, thus preventing proper treatment of electric transport. In previous calculations [27–29], a local approximation was adopted to reduce the computational efforts by ignoring the momentum dependence of the self-energies. This is equivalent to assigning independent electron baths for each local spin, as illustrated in Fig. 1(a). Under this approximation, only direct phase transitions are allowed, as shown in the inset of Fig. 1(b). To overcome this issue, we notice that the momentum convolution can be turned into simple multiplication in the coordinate space, $\Sigma_{b/\chi}(\mathbf{r}) \sim g_c(\mathbf{r}) G_{\chi/b}(\mathbf{r})$, which motivates us to develop an efficient algorithm based on the fast Fourier transform and to solve the above equations in coordinate space without approximation [37].

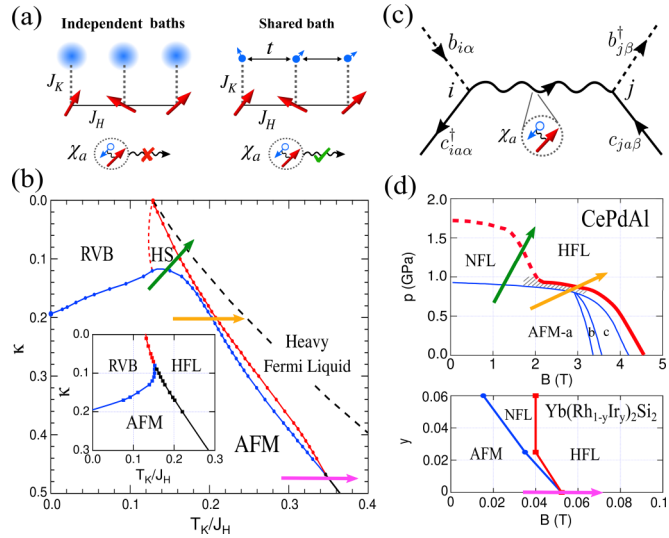

FIG. 1. (a) Illustration of the Kondo-Heisenberg model with independent electron baths where holons are not allowed to propagate on the lattice (left) and a shared bath in this work (right). (b) Theoretical phase diagram in the large-N limit on the κ and T_K/J_H plane, showing four phases: the Néel state (AFM), the resonating valence bond (RVB) state, the heavy Fermi liquid (HFL), and the intermediate holon state (HS). The RVB state may turn into the valence bond solid (VBS) at finite N. The AFM and HFL phase boundaries are separated for small κ but merge together for $\kappa \geqslant 0.47$. The intermediate HS region is missing under the local assumption (inset). The dashed line inside the HFL marks a transition from $\Delta \neq 0$ (short-range magnetic correlations) to $\Delta = 0$ (a local Fermi liquid). The arrows indicate different routes of quantum phase transitions. (c) The Feynman diagram of nonlocal Kondo scattering mediated by propagating holons. (d) Experimental phase diagrams of CePdAl [3] and Yb(Rh$_{1-y}$Ir$_y$)$_2$Si$_2$ [14]. The hatched area in the phase diagram of CePdAl marks the region with linear-in-T resistivity. The arrows mark possible correspondences with those in (b).

Figure 1(b) plots the resulting zero-temperature phase diagram on the κ and T_K/J_H plane, where $T_K = De^{-2D/J_K}$ is the single-ion Kondo temperature and D is the half bandwidth of conduction electrons. T_K/J_H is also called the Doniach ratio. The phase diagram contains four regions: the AFM Néel order, the resonating valence bond (RVB) state with a small electron Fermi surface, the HFL with a large electron Fermi surface, and the intermediate holon state (HS) with gapless spinon and holon excitations. Our result closely resembles the experimental phase diagram of CePdAl [Fig. 1(d)], showing different (narrow or wide) regions of intermediate NFL phase tuned by pressure and magnetic field [3]. The intermediate phase disappears for $\kappa > 0.47$ with weak quantum fluctuations, where the AFM and HFL transitions merge together to

give a single quantum critical point as in $YbRh_2Si_2$ tuned by Ir doping [14]. Inside the HFL, short-range magnetic correlations may vanish ($\Delta = 0$) at large T_K/J_H, and we enter a local Fermi liquid with independently screened spins.

The RVB, AFM, and HFL phases are already present in the local approximation and can be largely understood by two limits. In the Heisenberg limit ($J_K = 0$), the spins are decoupled from conduction electrons. At finite N, the RVB state will turn into the valence bond solid (VBS) state due to spinon confinement with the inclusion of monopoles [38,39]. The AFM Néel order is associated with spinon condensation. The transition between them marks a deconfined QCP with divergent spinon confinement length, where monopoles are irrelevant [40]. In this particular model, the VBS-AFM and RVB-AFM transitions are described by the same critical theory with gapless spinons and emergent U(1) gauge fields [41]. Our calculations reproduce the scaling of the staggered susceptibility $\chi_{st} \propto Te^{4\pi\rho_s/T}$ (ρ_s is the spin stiffness) in the renormalized classical regime above the Néel order and $\chi_{st} \propto T^{-2+\eta}$ in the quantum critical regime [42,43], with the anomalous dimension η approaching unity at the critical κ, reflecting deconfined free spinons [44]. In the limit of $\kappa \to 0$, both spinons and holons are localized, and the lattice physics is reduced to a collection of decoupled spins ($\Delta = 0$) undergoing independent Kondo screening beyond a critical T_K/J_H. For finite κ, the local approximation predicts direct transitions between three states, supporting local quantum criticality [45].

By contrast, our calculations with momentum-dependent quasiparticle self-energies reveal an intermediate phase (HS) with gapless spinon and holon excitations for $\kappa < 0.47$. Importantly, we obtain the correct zero-temperature AFM instability for both zero and finite J_K, in agreement with the Mermin-Wagner theorem [46], while the local approximation predicted incorrectly a finite-temperature transition for nonzero J_K [29]. Lattice propagations are crucial for both results, which yield a dispersive holon band and a holon Fermi surface determined by the poles of G_χ at the Fermi energy or, equivalently, the effective Kondo coupling, $J_K^*(\mathbf{p}) \equiv [J_K^{-1} + \mathrm{Re}\Sigma_\chi(\mathbf{p}, 0)]^{-1}$. Physically, the momentum dependence of $J_K^*(\mathbf{p})$ implies an unusual nonlocal and cooperative scattering process described by $J_K^*(\boldsymbol{r}_j - \boldsymbol{r}_i)c^\dagger_{ja\beta}b_{j\beta}b^\dagger_{i\alpha}c_{ia\alpha}$, in which a conduction hole and a spinon form a spinless quasibound state (holon) at $\boldsymbol{r}_i$, propagate to another site $\boldsymbol{r}_j$, and then unbind themselves [see Fig. 1(c)]. Such a "nonlocal Kondo effect" mediated by fractional quasiparticles underlies the emergent NFL state (HS) between antiferromagnetism and HFL and differs conceptually from an earlier proposal of partial Kondo screening in which local spins and electrons are both intact [18,23]. The presence of a holon Fermi surface may help further stabilize the deconfinement by coupling the surface to the U(1) gauge field at finite N and making monopole fluctuations irrelevant [47,48], while the gauge field is either "Higgsed" or confined in other three phases, forbidding fractional excitations at low temperatures.

The holon Fermi volume, $V_{\mathrm{FS}}^\chi = \mathcal{V}^{-1}\sum_{\mathbf{p}}\theta[-J_K^*(\mathbf{p})]$, is gauge invariant and evolves continuously in the intermediate state, as plotted in Fig. 2(b) for $\kappa = 0.1$. It satisfies the generalized Luttinger sum rule, $NV_{\mathrm{FS}}^c - V_{\mathrm{FS}}^\chi = n_c$, where V_{FS}^c is the Fermi volume of conduction electrons and n_c is the electron

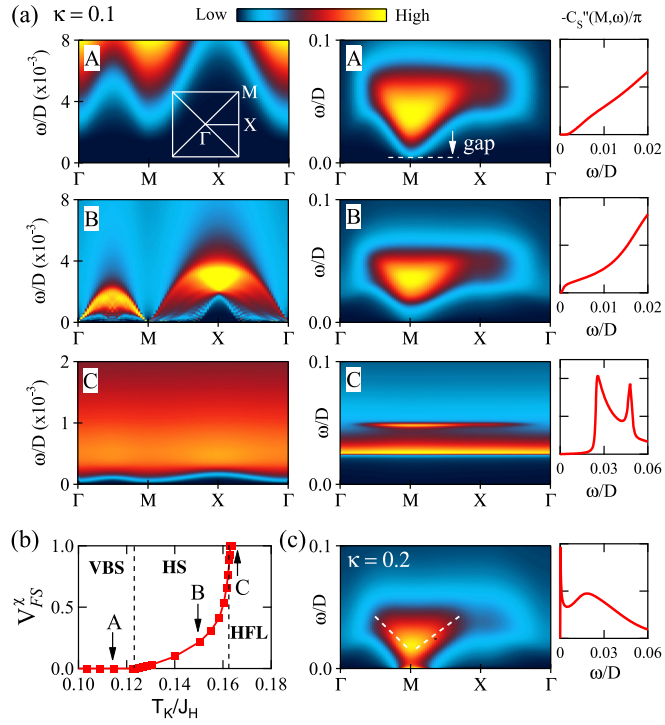

FIG. 2. (a) Holon (left panel) and spin (right panel) excitation spectra along the high-symmetry line of the Brillouin zone (inset) at $\kappa = 0.1$ for $T_K/J_H = 0.115$, 0.15, and 0.164 (from top to bottom) with different ground states as marked in (b). The color represents the intensity of the spectral functions $-C''_{n_\chi}(\mathbf{k}, \omega)/\pi$ and $-C''_S(\mathbf{k}, \omega)/\pi$. The spin spectra at M are also plotted for clarity. (b) Evolution of the holon Fermi volume V_{FS}^χ as a function of T_K/J_H at $\kappa = 0.1$. (c) The spin spectral function at $\kappa = 0.2$ and $T_K/J_H = 0.2$ at a low, but finite, T right above the AFM ground state. The white dashed lines are a guide to the eye.

number per channel (orbital) [30]. The sum rule reflects the electric charge conservation associated with the global U(1) symmetry: $\chi_{ia} \to \chi_{ia}e^{i\phi_a}$, $c_{i\alpha a} \to c_{i\alpha a}e^{-i\phi_a}$. As a result, the Fermi surface of conduction electrons is small ($NV_{\mathrm{FS}}^c = n_c$) in the RVB phase, large ($NV_{\mathrm{FS}}^c = n_c + 1$) in the HFL, and "partially" enlarged (or medium) in between, consistent with the calculated electron Fermi surface with $1/N$ correction [37]. For the local approximation, holons have no dispersion, and their Fermi volume is either zero or unity, thus preventing a partially enlarged electron Fermi surface. We note that the HS phase is different from the FL* phase discussed in Ref. [49]. The latter is characterized by decoupled spinons and a small electron Fermi surface, similar to our RVB state. It is also different from a conventional two-band metal with no fractional excitations and only (dispersive) intact f electrons [50].

More detailed information on the low-energy spin and charge excitations in the intermediate state can be extracted from the holon density-density correlation function $C_{n_\chi} = -\frac{1}{K}\langle n_\chi(\boldsymbol{r}_i, \tau)n_\chi(\boldsymbol{r}_j, \tau')\rangle_c$, where $n_\chi(\boldsymbol{r}_i, \tau) = \sum_a |\chi_{ia}(\tau)|^2$, and the dynamic spin structure factor $C_S = -\frac{1}{N}\langle S_i^z(\tau)S_j^z(\tau')\rangle_c$, with $S_i^z = \sum_\alpha \tilde{\alpha}b^\dagger_{i\alpha}b_{i\alpha}$. The subscript c denotes that only connected diagrams are considered. Figure 2(a) plots their imaginary parts in the energy-momentum space at $\kappa = 0.1$ for specially chosen values of

T_K/J_H. We find that both excitations are gapped in the RVB (panel A) and HFL (panel C) phases. In the intermediate state (panel B), the holons become gapless around Γ and M, corresponding to particle-hole pairs from the same or different parts of the holon Fermi surface. With increasing T_K/J_H, the holon bands D_χ become increasingly narrow, implying a heavy effective mass as large as $m^*_\chi/m_e \propto D/D_\chi \approx 10^4$ near the HFL boundary. Across the boundary, the holon Fermi surface vanishes in the HFL state. Accordingly, conduction electrons achieve a large Fermi surface following the Luttinger sum rule. The spin excitation spectra in the intermediate state are also gapless but highly damped. For the square lattice model in the Heisenberg limit, the spectra are sharply defined but gapped outside of the AFM phase. Here the coupling with holons smears out the gap and results in gapless, but damped, spin excitations. For comparison, Fig. 2(c) shows the results for $\kappa = 0.2$ at low, but finite, temperature above the AFM ground state. We find a sharp peak near zero energy that is the precursor of spinon condensation. This distinguishes the spinon dynamics inside the intermediate phase. At $\kappa = 0.48$, the AFM QCP marks a direct transition to the HFL and features both critical spinons and heavy holons [37]. Given the gapless charge and spin excitations, the Kondo screening may exist in a critical way inside the HS. Its difference from the fully Kondo screened HFL may also be reflected in two-particle correlation functions [51], which unfortunately require two-loop diagrams beyond our numerical capability.

Thus, the phase diagram for $\kappa > 0.1$ is largely controlled by the interplay of a deconfined AFM QCP and a transition to the large electron Fermi surface. At finite temperature, one may further expect a crossover line connected to the renormalized classical regime in the Heisenberg limit above the AFM order and a delocalization line associated with the transition to the large electron Fermi surface. In between, irrespective of an intermediate state or a QCP at zero temperature, there always exists a paramagnetic region with short-lived spinon and holon excitations and a partially enlarged electron Fermi surface. This provides a candidate microscopic interpretation of the two-fluid model with a coexistent spin liquid and heavy quasiparticles [52,53]. The partially enlarged electron Fermi surface evolves with temperature, supported recently by angle-resolved photoemission spectroscopy (ARPES) [54] and ultrafast optical pump-probe spectroscopy [55] in $CeCoIn_5$. The fact that it varies continuously and is "nearly large" in the vicinity of the single QCP for large κ might help resolve the recent controversy for $YbRh_2Si_2$, in which, contrary to the usual expectation based on the change in the Hall coefficient [5], ARPES reported a large Fermi surface above the antiferromagnetism (70 mK) [56]. Even deep on the AFM side, "band bending" has been observed in paramagnetic $CeRhIn_5$ [57]. The crossover in the Hall coefficient might be explained if holon contributions are taken into consideration [58–60]. The presence of deconfined holons is a peculiar feature of the intermediate region in our theory whose consequences have yet to be fully elaborated. In the AFM phase at zero temperature, a small electron Fermi surface is always expected due to spinon condensation.

Some of the physical properties in the intermediate region can be approximately captured by the large-N limit.

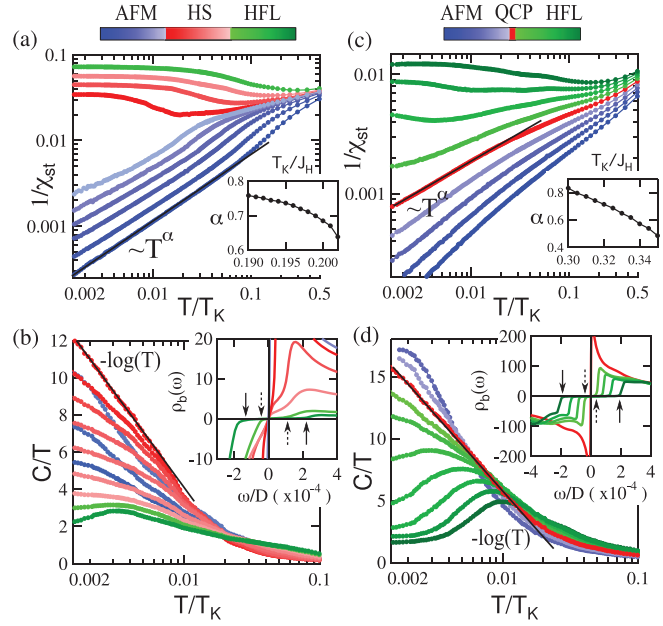

FIG. 3. Temperature dependence of (a) the inverse staggered susceptibility and (b) the specific heat coefficient at $\kappa = 0.2$ for different values of T_K/J_H. The colors distinguish the AFM (blue), HS (red), and HFL (green) regions. The inset in (a) shows the power-law exponent α as a function of T_K/J_H on the AFM side, and that in (b) compares the low-temperature spinon density of states in the HS and HFL regions. The arrows mark the gap edges. (c) and (d) Same as (a) and (b), but at $\kappa = 0.48$, where the red color denotes the QCP.

Figure 3 plots the calculated staggered magnetic susceptibility χ_{st} and specific heat coefficient C/T at $\kappa = 0.2$ and 0.48. In both cases, we see $\chi_{st} \sim T^{-\alpha}$ on the AFM side and $C/T \sim -\ln T$ at the AFM QCP, typical of NFL. The exponent α varies monotonically with T_K/J_H and drops rapidly near the AFM QCP (roughly 0.5 at $\kappa = 0.48$). Its value is much smaller than that of the Heisenberg model, reflecting the presence of additional holon excitations. Its nonuniversality seems to be consistent with experimental observations, where α varies from 1/3 in $UCu_{5-x}Pd_x$ [61] to 0.51 in $Ce(Ru_{1-x}Fe_x)_2Ge_2$ [62] to 0.75 in $CeCu_{5.9}Au_{0.1}$ [11]. Inside the HFL, C/T shows a broad maximum at finite temperature. This difference may be understood from the insets in Figs. 3(b) and 3(d), where the spinon density of states is singular at the AFM QCP but gapped in the HFL. Inside the intermediate state, the spinon density of states is gapless but nonsingular, and C/T keeps growing with decreasing temperature, reflecting nonuniversal NFL behaviors, as observed in CePdAl [3].

It remains to be seen how transport properties might be affected when the electron self-energy is included at finite N. A linear-in-T resistivity has been proposed to arise either from critical holons [28] or due to spinon scattering with vanishing holon velocity [31]. This might be true near the AFM QCP but must not be extended to the whole intermediate region where spinon and holon dynamics are not always critical, even for frustrated Kondo lattices. Indeed, the linear-in-T resistivity was observed over only a narrow region of the intermediate phase in CePdAl [3]. Its appearance is probably associated

with the distorted kagome structure, calculations of which require more auxiliary fields and will be left for future work.

The intermediate phase has also been observed in other compounds, including $YbRh_2Si_2$ with Ir or Ge doping [14,15] and YbAgGe under field [63]. These compounds adopt different crystal structures, suggesting that the intermediate phase is not a phenomenon solely of frustrated Kondo lattices. Large spin/orbital degeneracy and low dimensionality may also introduce strong quantum fluctuations [64]. Of course, the details of the phase diagram may be altered by finite-N corrections including gauge fluctuations. Nevertheless, our approach allows for the possibility of the intermediate NFL state, which is an advance beyond the local approximation. Key features distinguishing our theory from the conventional Hertz-Millis theory include the partially enlarged electron Fermi surface with an intermediate Fermi wave vector [30], the existence of multiple charge carriers, and possibly singular charge fluctuations [7,28]. More elaborate studies along this line may lead to a better understanding of Kondo lattice physics.

This work was supported by the National Key R&D Program of China (Grant No. 2017YFA0303103), the National Natural Science Foundation of China (Grants No. 12174429, No. 11774401, No. 11974397), and the Strategic Priority Research Program of the Chinese Academy of Sciences (Grant No. XDB33010100).

[1] Q. Si and F. Steglich, Science **329**, 1161 (2010).
[2] Y.-F. Yang, D. Pines, and G. Lonzarich, Proc. Natl. Acad. Sci. USA **114**, 6250 (2017).
[3] H. Zhao, J. Zhang, M. Lyu, S. Bachus, Y. Tokiwa, P. Gegenwart, S. Zhang, J. Cheng, Y.-F. Yang, G. Chen, Y. Isikawa, Q. Si, F. Steglich, and P. Sun, Nat. Phys. **15**, 1261 (2019).
[4] J. Custers, P. Gegenwart, H. Wilhelm, K. Neumaier, Y. Tokiwa, O. Trovarelli, C. Geibel, F. Steglich, C. Pépin, and P. Coleman, Nature (London) **424**, 524 (2003).
[5] S. Paschen, T. Lühmann, S. Wirth, P. Gegenwart, O. Trovarelli, C. Geibel, F. Steglich, P. Coleman, and Q. Si, Nature (London) **432**, 881 (2004).
[6] S. Friedemann, N. Oeschler, S. Wirth, C. Krellner, C. Geibel, F. Steglich, S. Paschen, S. Kirchner, and Q. Si, Proc. Natl. Acad. Sci. USA **107**, 14547 (2010).
[7] L. Prochaska, X. Li, D. C. MacFarland, A. M. Andrews, M. Bonta, E. F. Bianco, S. Yazdi, W. Schrenk, H. Detz, A. Limbeck, Q. Si, E. Ringe, G. Strasser, J. Kono, and S. Paschen, Science **367**, 285 (2020).
[8] T. Park, F. Ronning, H. Q. Yuan, M. B. Salamon, R. Movshovich, J. L. Sarrao, and J. D. Thompson, Nature (London) **440**, 65 (2006).
[9] H. Shishido, R. Settai, H. Harima, and Y. Ōnuki, J. Phys. Soc. Jpn. **74**, 1103 (2005).
[10] H. v. Löhneysen, S. Mock, A. Neubert, T. Pietrus, A. Rosch, A. Schröder, O. Stockert, and U. Tutsch, J. Magn. Magn. Mater. **177–181**, 12 (1998).
[11] A. Schröder, G. Aeppli, R. Coldea, M. Adams, O. Stockert, H. v. Löhneysen, E. Bucher, R. Ramazashvili, and P. Coleman, Nature (London) **407**, 351 (2000).
[12] M. Klein, A. Nuber, F. Reinert, J. Kroha, O. Stockert, and H. v. Löhneysen, Phys. Rev. Lett. **101**, 266404 (2008).
[13] M. Klein, J. Kroha, H. v. Löhneysen, O. Stockert, and F. Reinert, Phys. Rev. B **79**, 075111 (2009).
[14] S. Friedemann, T. Westerkamp, M. Brando, N. Oeschler, S. Wirth, P. Gegenwart, C. Krellner, C. Geibel, and F. Steglich, Nat. Phys. **5**, 465 (2009).
[15] J. Custers, P. Gegenwart, C. Geibel, F. Steglich, P. Coleman, and S. Paschen, Phys. Rev. Lett. **104**, 186402 (2010).
[16] Q. Si, Phys. B (Amsterdam, Neth.) **378**, 23 (2006).
[17] P. Coleman and A. H. Nevidomskyy, J. Low. Temp. Phys. **161**, 182 (2010).
[18] J. H. Pixley, R. Yu, and Q. Si, Phys. Rev. Lett. **113**, 176402 (2014).
[19] T. Tomita, K. Kuga, Y. Uwatoko, P. Coleman, and S. Nakatsuji, Science **349**, 506 (2015).
[20] A. Georges, G. Kotliar, W. Krauth, and M. J. Rozenberg, Rev. Mod. Phys. **68**, 13 (1996).
[21] L. C. Martin and F. F. Assaad, Phys. Rev. Lett. **101**, 066404 (2008).
[22] D. Tanasković, K. Haule, G. Kotliar, and V. Dobrosavljević, Phys. Rev. B **84**, 115105 (2011).
[23] T. Sato, F. F. Assaad, and T. Grover, Phys. Rev. Lett. **120**, 107201 (2018).
[24] J. Rech, P. Coleman, G. Zarand, and O. Parcollet, Phys. Rev. Lett. **96**, 016601 (2006).
[25] E. Lebanon, J. Rech, P. Coleman, and O. Parcollet, Phys. Rev. Lett. **97**, 106604 (2006).
[26] E. Lebanon and P. Coleman, Phys. Rev. B **76**, 085117 (2007).
[27] Y. Komijani and P. Coleman, Phys. Rev. Lett. **120**, 157206 (2018).
[28] Y. Komijani and P. Coleman, Phys. Rev. Lett. **122**, 217001 (2019).
[29] J. Wang, Y.-Y. Chang, C.-Y. Mou, S. Kirchner, and C.-H. Chung, Phys. Rev. B **102**, 115133 (2020).
[30] P. Coleman, I. Paul, and J. Rech, Phys. Rev. B **72**, 094430 (2005).
[31] C. Pépin, Phys. Rev. Lett. **94**, 066402 (2005).
[32] R. Flint and P. Coleman, Phys. Rev. B **79**, 014424 (2009).
[33] T. N. De Silva, M. Ma, and F.-C. Zhang, Phys. Rev. B **66**, 104417 (2002). We have chosen a constant $\zeta \approx 0.33$ to remove possible first-order transitions for all values of κ in this work. A smaller $\zeta \approx 0.001$ was used for the one-dimensional ferromagnetic Kondo-Heisenberg model [27].
[34] O. Parcollet and A. Georges, Phys. Rev. Lett. **79**, 4665 (1997).
[35] N. Read and S. Sachdev, Phys. Rev. Lett. **66**, 1773 (1991).
[36] X.-G. Wen, Phys. Rev. B **65**, 165113 (2002).
[37] See Supplemental Material at http://link.aps.org/supplemental/10.1103/PhysRevB.104.165120 for more theoretical and numerical details.
[38] N. Read and S. Sachdev, Phys. Rev. Lett. **62**, 1694 (1989).
[39] N. Read and S. Sachdev, Phys. Rev. B **42**, 4568 (1990).
[40] T. Senthil, A. Vishwanath, L. Balents, S. Sachdev, and M. P. A. Fisher, Science **303**, 1490 (2004).
[41] T. Senthil, L. Balents, S. Schdev, A. Vishwanath, and M. P. A. Fisher, J. Phys. Soc. Jpn. **74**, 1 (2005).
[42] S. Chakravarty, B. I. Halperin, and D. R. Nelson, Phys. Rev. B **39**, 2344 (1989).

[43] A. V. Chubukov, S. Sachdev, and J. Ye, Phys. Rev. B **49**, 11919 (1994).
[44] R. K. Kaul and S. Sachdev, Phys. Rev. B **77**, 155105 (2008).
[45] Q. Si, S. Rabello, K. Ingersent, and J. L. Smith, Nature (London) **413**, 804 (2001).
[46] N. D. Mermin and H. Wagner, Phys. Rev. Lett. **17**, 1133 (1966).
[47] M. Hermele, T. Senthil, M. P. A. Fisher, P. A. Lee, N. Nagaosa, and X.-G. Wen, Phys. Rev. B **70**, 214437 (2004).
[48] S.-S. Lee, Phys. Rev. B **78**, 085129 (2008).
[49] T. Senthil, S. Sachdev, and M. Vojta, Phys. Rev. Lett. **90**, 216403 (2003).
[50] T. Senthil, M. Vojta, and S. Sachdev, Phys. Rev. B **69**, 035111 (2004).
[51] P. Chalupa, T. Schäfer, M. Reitner, D. Springer, S. Andergassen, and A. Toschi, Phys. Rev. Lett. **126**, 056403 (2021).
[52] Y.-F. Yang and D. Pines, Proc. Natl. Acad. Sci. USA **109**, E3060 (2012).
[53] Y.-F. Yang, Rep. Prog. Phys. **79**, 074501 (2016).
[54] Q. Y. Chen *et al.* Phys. Rev. B **96**, 045107 (2017).
[55] Y. P. Liu, Y. J. Zhang, J. J. Dong, H. Lee, Z. X. Wei, W. L. Zhang, C. Y. Chen, H. Q. Yuan, Y.-F. Yang, and J. Qi, Phys. Rev. Lett. **124**, 057404 (2020).
[56] K. Kummer, S. Patil, A. Chikina, M. Güttler, M. Höppner, A. Generalov, S. Danzenbächer, S. Seiro, A. Hannaske, C. Krellner, Yu. Kucherenko, M. Shi, M. Radovic, E. Rienks, G. Zwicknagl, K. Matho, J. W. Allen, C. Laubschat, C. Geibel, and D. V. Vyalikh, Phys. Rev. X **5**, 011028 (2015).
[57] Q. Y. Chen, D. F. Xu, X. H. Niu, R. Peng, H. C. Xu, C. H. P. Wen, X. Liu, L. Shu, S. Y. Tan, X. C. Lai, Y. J. Zhang, H. Lee, V. N. Strocov, F. Bisti, P. Dudin, J.-X. Zhu, H. Q. Yuan, S. Kirchner, and D. L. Feng, Phys. Rev. Lett. **120**, 066403 (2018).
[58] J. Zhang, H. Zhao, M. Lv, S. Hu, Y. Isikawa, Y.-F. Yang, Q. Si, F. Steglich, and P. Sun, Phys. Rev. B **97**, 235117 (2018).
[59] S. Nair, S. Wirth, S. Friedemann, F. Steglich, Q. Si, and A. J. Schofield, Adv. Phys. **61**, 583 (2012).
[60] P. Coleman, C. Pépin, Q. Si, and R. Ramazashvili, J. Phys.: Condens. Matter **13**, R723 (2001).
[61] M. C. Aronson, M. B. Maple, R. Chau, A. Georges, A. M. Tsvelik, and R. Osborn, J. Phys.: Condens. Matter **8**, 9815 (1996).
[62] W. Montfrooij, M. C. Aronson, B. D. Rainford, J. A. Mydosh, A. P. Murani, P. Haen, and T. Fukuhara, Phys. Rev. Lett. **91**, 087202 (2003).
[63] G. M. Schmiedeshoff, E. D. Mun, A. W. Lounsbury, S. J. Tracy, E. C. Palm, S. T. Hannahs, J.-H. Park, T. P. Murphy, S. L. Bud'ko, and P. C. Canfield, Phys. Rev. B **83**, 180408(R) (2011).
[64] B. Coqblin and J. R. Schrieffer, Phys. Rev. **185**, 847 (1969).